

C–C Bond Scission in Ethane Hydrogenolysis

Andrew V. Zeigarnik,^{*,†} Raúl E. Valdés-Pérez,[‡] and Olga N. Myatkovskaya[†]

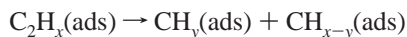
Laboratory of Chemical Kinetics and Catalysis, Lomonosov Academy of Fine Chemical Technology, Moscow 117571, Russia, and Computer Science Department, Carnegie Mellon University, Pittsburgh, Pennsylvania 15213

Received: March 22, 2000; In Final Form: July 5, 2000

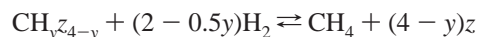
C–C bond scission steps are often considered rate-determining in ethane hydrogenolysis. This paper is devoted to the calculations of the activation energies of these steps using the unity bond index–quadratic exponential potential method, formerly known as the bond-order conservation–Morse potential method. Binding energies of atomic carbon with groups VIII and IB metals Ni(111), Pd(111), Pt(111), Rh(111), Ru(0001), Ir(111), Fe(110), Cu(111), and Au(111) are estimated from experimental data on the chemisorption of various species on these surfaces. The resulting estimates are corrected taking into account DFT data on CH_x binding energies. The strengths of carbon binding to the surfaces allow arranging the metals into the following series: Cu(111) < Au(111) < Pd(111) < Ru(0001) < Pt(111) ≈ Ni(111) < Rh(111) < Ir(111) < Fe(110). The values of carbon binding energies range from 122.9 kcal/mol for Cu(111) to 192.5 kcal/mol for Fe(110). The activities of these surfaces toward C–C bond scission increase in the same series.

1. Introduction

The exact mechanism of ethane hydrogenolysis is still unknown, although most researchers agree that the Sinfelt–Taylor mechanism is correct for many group VIII metals.^{1–14} Some believe that this mechanism is incorrect or inapplicable to all metal surfaces.¹⁵ The Sinfelt–Taylor mechanism involves the following steps: (1) chemisorption of H₂; (2) ethane dehydrogenation on a catalyst surface to form adsorbed C₂H_x species; (3) C–C bond scission in C₂H_x ($x = 5–0$) to form CH_y ($y = 0, 1, \dots, x$)



(4) CH_y hydrogenation to form methane, which then desorbs from the surface. Steps of the third type are most frequently assumed to be rate-determining, while the others are pseudo-equilibrium steps. In this mechanism, all of the C₂H_x or CH_y species are at equilibrium with either reactants or products of the reaction:



where z is an active site.

Sinfelt generalized the data on ethane hydrogenolysis in review papers.^{1,2} A main argument in favor of the above mechanism is that hydrocarbons chemisorb on metallic surfaces at substantially lower temperatures than those needed for hydrogenolysis. As this takes place, hydrogen is evolved into the gas phase. Further evidence is the data on H/D exchange under hydrogenolysis conditions, which suggest that C–H bonds are more reactive than C–C bonds, although the latter are

weaker by ~10 kcal/mol. The factors determining the heights of the activation barriers are the strengths of the C–H and C–C bonds and the binding energies (chemisorption heats) of intermediate species to metal surfaces.

Sinfelt's kinetic analysis of ethane hydrogenolysis within the framework of the proposed mechanism for various transition metals supported on SiO₂ has led to the conclusion that the number of hydrogen atoms in the C₂H_x fragments in which the C–C bond cleaves differs from one surface to another (see Table 1). This analysis assumes a lack of competition between ethane and hydrogen for active sites on the surface; Boudart criticized such an approach.¹⁶

A slightly different version of the C–C bond scission step was considered in several papers:^{2,17,18}



For instance, Mahaffy and Hansen suggested a rate-determining step of a slightly different type for the reaction over iridium films:



Chen and Goodwin¹⁸ proposed the same rate-determining step for ethane hydrogenolysis over Ru/SiO₂.

Frennet et al.¹⁵ criticized the idea that C–C bond scission is the rate-determining step for all transition-metal surfaces. They believe that the steps of CH_x hydrogenation can also be rate-determining, and they provided evidence from data on deuterium exchange in methane. They concluded that (i) deuterium exchange in ethane always occurs at substantially lower temperatures than hydrogenolysis (with the exception of iron and cobalt), (ii) the rates of deuterium exchange and hydrogenolysis are very close on W, Ni, Rh, Ru, Re, and Pd, while the rate of hydrogenolysis is somewhat lower on Ni, Re, and Pd and somewhat higher on Rh, Ru, and W, (iii) deuterium exchange in methane is much slower on Fe, Co, and Cu, for which methane adsorption is slow or does not occur at all, as

* To whom correspondence should be addressed. E-mail: azeigarn@cs.cmu.edu.

[†] Lomonosov Academy of Fine Chemical Technology.

[‡] Carnegie Mellon University. E-mail: valdes@cs.cmu.edu.

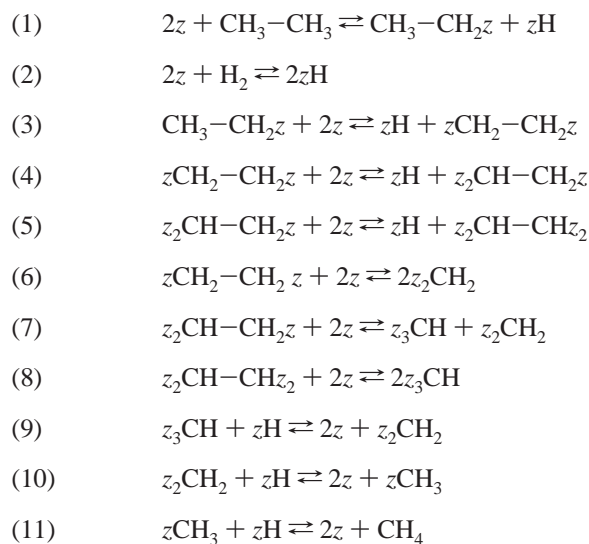
TABLE 1: Immediate Precursors of C–C Bond Scission in Ethane Hydrogenolysis over Different Surfaces^a

catalyst/ surface	precursor of C–C bond scission (stoichiometry or structure)	ref
Co/SiO ₂	CH ₂ CH ₂	1–3
Co/SiO ₂	CH ₂ CH ₂ or CH ₂ CH	4
Ni/SiO ₂	CHCH	1–3
Ni/SiO ₂	C ₂ H ₀	12
Ni/TiO ₂	C ₂ H ₄	14
Ni powder	C ₂ H _x , x < 4	6
Ru/SiO ₂	CHCH	1–3
Ru/SiO ₂	C ₂ H ₃	8
Ru/TiO ₂	C ₂ H ₂	14
Ir(110)-(1×2)	C ₂ H ₂	10
Ir(111)	C ₂ H ₄	10
Ir/η–Al ₂ O ₃	CHCH	13
Ir/SiO ₂	CHCH	1–3
Ir/SiO ₂	CH ₂ CH ₂ or CH ₂ CH	4
Os/SiO ₂	CHCH	1–3
Os/TiO ₂	C ₂ H ₄	14
Pd/SiO ₂	C ₂ H ₀	1–3
Pd/SiO ₂	CH ₂ CH ₂ or CH ₂ CH	4
Pd/TiO ₂	C ₂ H ₂	14
Pt(111)	C ₂ H ₄ or C ₂ H ₃ (possibly CH ₃ C)	11
Pt/η–Al ₂ O ₃	C ₂ H ₀ , CHC, or CH ₃ C	13
Pt/SiO ₂	C ₂ H ₀	1–3
Pt/SiO ₂	CHCH or CH ₃ CH ₂	9
Pt/SiO ₂	CH ₂ CH ₂ or CH ₂ CH	4
Rh/SiO ₂	C ₂ H ₀	1–3
Rh/TiO ₂	C ₂ H ₀	14

^a Summary of the available literature data.

in the case of Cu, and (iv) on a platinum surface, hydrogenolysis is slower than deuterium exchange.

Dumesic and co-workers⁴ modeled ethane hydrogenolysis over Pt, Pd, Ir, and Co supported on SiO₂. They proposed the following mechanism:



This mechanism assumes that the immediate precursors of C–C bond scission are the fragments $\text{--CH}_2\text{--CH}_2\text{--}$, $\text{=CH--CH}_2\text{--}$, and =CH--CH= . Three pathways (routes) were considered: A (steps 1–3, 6, 10, and 11), B (steps 1–4, 7, and 9–11), and C (steps 1–5 and 8–11). Pathway C and C–C scission in C₂H₂ are not operative for the four cited metals. Either pathway A or pathway B may dominate depending on the metal and conditions.

Ko and Garten¹⁴ published evidence for strong metal–support interactions under hydrogenolysis conditions. They studied this

reaction over a series of metal catalysts, Fe, Co, Ni, Ru, Rh, Pd, Os, Ir, and Pt, supported on TiO₂. Their comparison to Sinfelt’s¹ data for the same metals supported on SiO₂ revealed that the use of a different support alters the catalytic activity pattern. An analysis similar to Sinfelt’s suggested that the degree of ethane dehydrogenation before C–C bond scission also changes when one switches from SiO₂ to TiO₂. These authors compared two series of specific activities of the group VIII metals, one of which corresponds to the SiO₂ support (according to Sinfelt’s data), Os > Ru > Ni > Rh > Ir > Co > Fe > Pt > Pd, and the other is for TiO₂,¹⁴ Ru > Os > Rh > Ni > Ir > Co > Pd > Pt ≈ Fe.

In both cases, Ru, Os, Rh, and Ni are more active and Co, Fe, Pt, and Pd are less active. Iridium shows moderate activity. Supported metal surfaces may show different activities due to the participation of the support in the reaction mechanism or due to other reasons. The activities of different planes of single-crystal surfaces may also differ. Ethane hydrogenolysis was found to be structure-sensitive as indicated in the activity series reported by Rodriguez and Goodman.¹⁹ Single-crystal surfaces can be arranged in the following series according to the turnover frequency: Ir(110)-(1×2) > Ir(111) > Ru(0001) > Ni(100) > Re(0001) > Ni(111) > W(100) > Pt(111). As can be seen, iridium planes become more active than nickel and platinum planes, but platinum preserves its relative position in the activity series.

Table 1 summarizes various proposals regarding precursors of C–C bond scission for different surfaces. These data are incomplete and somewhat controversial. In most cases, the Sinfelt–Taylor mechanism was assumed when the most probable precursors were inferred. However, it is clear that accurate kinetic models for simulating the process should involve several possible C–C bond scission precursors.

In this work, we carried out calculations to identify the most probable precursors by tracing the trends in activation energies for these steps on a larger set of metal surfaces than has been considered before. These activation energies correlate with the values of the energies of atomic carbon binding to surfaces, which are also very important for catalysis. Although the ethane hydrogenolysis activity series for metals is known from experiments, theoretical support is desirable, since experimental data may be inaccurate. Hence, a combination of experimental and theoretical evidence is needed to gain reliable knowledge of relative activities and carbon binding strengths over many metal surfaces, which is important for both theory and practice.

For this purpose, we used the unity bond index–quadratic exponential potential (UBI–QEP) method, formerly known as the bond-order conservation–Morse potential (BOC–MP) method.^{20,21} The calculation scheme was as follows: (i) Using published experimental data, estimate the binding energies of atomic carbon on low-index planes of transition-metal single-crystal surfaces. (ii) Using the data obtained at the first stage, calculate the binding energies for the C₁–C₂ species on these surfaces. (iii) Using the data obtained at the second stage, calculate the activation energies of C–C bond scission. In all calculations, we assume the zero-coverage limit for surfaces. This condition corresponds to the experimental data that we use.

When UBI–QEP theory is employed to calculate the activation energies of elementary steps in heterogeneous catalysis, the usual approach is based on conjecturing the strengths of metal–X bonds (X = C, H, O, N, etc.) and comparing the calculated values to the available experimental data. In this paper, we proceed in a bootstrap fashion: we first calculate the

strengths of metal–carbon bonds *on the basis of the available data on binding energies* (stage i), and then fill in the values of the missing binding energies (stage ii). To the best of our knowledge, such a method has never before been applied to a large set of metal surfaces.

2. Theoretical Method

The main source for estimating the binding energies of carbon Q_C is the data on the heats of CO adsorption (Q_{CO}). The metal–carbon bond energy D_{MC} ($=Q_{0C}$) is related to the heat of CO adsorption Q_{CO} by the following formula:

$$Q_{CO} = \frac{D_{MC}^2}{D_{MC} + D_{CO}} \quad (1a)$$

where D_{CO} is the C–O bond energy (257 kcal/mol). D_{MC} and Q_C are related by the formula

$$Q_{0C} \equiv D_{MC} = \frac{Q_C}{2 - 1/n} \quad (2a)$$

In formula 2a, n is the number of metal atoms to which carbon binds. If carbon adsorbs on the (111) fcc or (0001) hcp surface, then $n = 3$.

In the general case

$$Q_{0A} = \frac{Q_A}{2 - 1/n} \quad (2)$$

where Q_{0A} and Q_A are, respectively, the energy of the metal–A bond and the binding energy (chemisorption heat) of A.

For monocoordinated chemisorbed AB molecules that bond to the surface via atom A, the choice of appropriate formula depends on the assumed strength of adsorption on the metal surface.

Strong binding of an adsorbate X ($X = CH_3CH$, CH_3C , CH_2 , CH) with the surface via the A atom (in our case, A is carbon) corresponds to the formula

$$Q_X = \frac{Q_A^2}{Q_A + D_{AB}} \quad (1)$$

D_{AB} is the sum of bond energies between the atom that binds to the surface and the rest of the molecule. For CH_3CH , CH_3C , CH_2 , and CH , $D_{AB} = 173$, 83 , 183 , and 81 kcal/mol, respectively; $Q_A = Q_C$. The data on bond energies are taken from ref 22.

If binding is of medium strength,^{20,21} then the following formula should apply:

$$Q_X = 0.5 \left(\frac{Q_{0A}^2}{Q_{0A}/n + D_{AB}} + \frac{Q_A^2}{Q_A + D_{AB}} \right) \quad (3)$$

$X = CH_3CH_2$ and CH_3 and $D_{AB} = 283$ and 293 kcal/mol, respectively.

The binding energies of dicoordinated AB molecules bound to the surface via atoms A and B ($M-A \cdots B-M$) are calculated using the formula^{20,21}

$$Q_X = \frac{ab(a+b) + D_{AB}(a-b)^2}{ab + D_{AB}(a+b)} \quad (4)$$

where

$$a = Q_{0A}^2 \frac{Q_{0A} + 2Q_{0B}}{(Q_{0A} + Q_{0B})^2} \quad (5)$$

and

$$b = Q_{0B}^2 \frac{Q_{0B} + 2Q_{0A}}{(Q_{0A} + Q_{0B})^2} \quad (6)$$

In formula 4, D_{AB} is the energy of the C–C bond: $D_{CH_2-CH} = 157$, $D_{CH_2=C} = 165$, and $D_{CH=C} = 178$ kcal/mol.²⁰ The values Q_{0A} and Q_{0B} in formulas 5 and 6 are calculated using the equation (where in our case, A and B are carbon atoms)

$$Q_{0B} = \frac{Q_{0C}^2}{Q_{0C} + D_i} \quad (7)$$

where D_i is the energy required for the scission of bonds between the contact atom and other atoms in fragment A or B. Below are the values of D_i (kcal/mol) for different adsorbates taking into account the partitioning of bond energies in the molecules:²⁰ $D_{CH_2} = 183$ kcal/mol and $D_{CH} = 81$ kcal/mol.

For homonuclear adsorbates A_2 ($-CH=CH-$, $-C \equiv C-$, and $-CH_2-CH_2-$), formula 4 can be simplified:

$$Q_{A_2} = \frac{9Q_{0A}^2}{6Q_{0A} + 16D_{A_2}} \quad (8)$$

For CH_2CH_2 , $CHCH$, and CC , D_{A_2} is the energy of C–C bond scission between CH_2 , CH , and C , respectively, and the rest of the molecule in the gas phase: $D_{CH_2-CH_2} = 355$, $D_{CH=CH} = 311$, and $D_{C-C} = 145$ kcal/mol. $Q_{0A} = Q_{0C}$ is the binding energy of a contact atom.

The UBI–QEP method enables calculation of the activation energies of reactions on surfaces. For the dissociation reaction



the following equation is used:

$$E = 0.5 \left(\Delta H + \frac{Q_A Q_B}{Q_A + Q_B} \right) \quad (9)$$

where ΔH is the enthalpy of reaction on the metal surface calculated from the thermodynamic cycle *desorption* \rightarrow *gas-phase reaction* \rightarrow *adsorption*:

$$\Delta H = Q_{AB} + D - Q_A - Q_B \quad (10)$$

In this case, D is the enthalpy of the analogous gas-phase reaction estimated from the bond energies:

$$D = D_{AB} - D_A - D_B \quad (11)$$

The activation energy of the reverse reaction is calculated using the condition

$$E_{backward} = E_{forward} - \Delta H \quad (12)$$

If a calculated activation energy is negative, then a thermodynamic correction should be introduced: the negative activation

TABLE 2: Binding Energies of Carbon

	Cu(111)	Ni(111)	Pd(111)	Pt(111)	Rh(111)	Ru(111)	Ir(111)	Fe(110)	Au(111)
Q_C^a	107.0	171.3	189.2	184.8	176.8	166.6	192.7	192.5	131.2
Q_C^b	122.9	181.0	170.1	180.6	183.0	175.1	189.9		127.8

^a Calculated from the experiment. ^b Corrected values (see text for details).^{73,74}

energy is set to zero, and the activation energy of the reverse reaction is set to the absolute value of the reaction enthalpy.

3. Results and Discussion

3.1. Carbon Binding Energies. The binding energy of atomic carbon is an important characteristic of surfaces. The UBI–QEP model requires this value as input. Bradford showed that this value is also pivotal to determine the catalyst efficiency, chain growth probability, and selectivity to C₂ and higher hydrocarbons in CH₄ homologation over supported metal catalysts.²³ The most comprehensive source of carbon binding energies is a chapter by Benziger in *Metal-Surface Reaction Energetics*.²⁴ This paper revises these data on the basis of the information available to date and calculations of carbon binding energies from adsorbate binding energies.

3.1.1. Cu(111). The binding energy of carbon for Cu(111) is known to be lower than for the group VIII metals. An experimental value that can be used to calculate the binding energy of a carbon atom is $Q_{\text{CH}_3} = 29 \pm 2$ kcal/mol,²⁵ which corresponds to $Q_C \approx 128.8$ kcal/mol. The range of surface coverages to which this value is applicable is uncertain, but since Q_{CH_3} should decrease with the coverage, $Q_C = 128.8$ kcal/mol can be considered a lower limit. On the other hand, $Q_{\text{CO}} = 11.9$ kcal/mol²⁶ predicts a lower value of $Q_C = 102.6$ kcal/mol for coverages lower than 1/3 monolayer (ML). The surface that is most similar to Cu(111) is Cu(100), for which the following experimental values are available: $Q_{\text{CO}} = 13.2 \pm 0.3$ kcal/mol,²⁷ $Q_{\text{CO}} = 13.5$ kcal/mol,²⁸ $Q_{\text{C}_2\text{H}_4} = 8 \pm 2$ kcal/mol,²⁹ $Q_{\text{C}_2\text{H}_5} = 33 \pm 6$ kcal/mol.³⁰ The data for the (100) plane can also be used, although with care, since ethane hydrogenolysis is a structure-sensitive reaction.^{19,31} Binding energies for alkyl radicals and ethylene cited here refer to uncertain coverage ranges and give much higher values. Because in further parametrization CO is the main reference adsorbate, we took only three values for CO adsorption, which predict an average value of $Q_C = 107.0$ kcal/mol.

3.1.2. Ni(111). In most of the previous UBI–QEP calculations for Ni(111), the binding energy of carbon was set to 171 kcal/mol.^{20,21,32–35} This is a well-calibrated value which is close to the binding energy of carbon on Ni(100): $Q_C = 171.5$ kcal/mol.³⁶

For CO/Ni(111), the following binding energies were reported: 29.4 (for coverages below 0.1 ML) and 26.5 (for coverages between 0.1 and 0.3 ML),³⁷ 35.6,³⁸ 31 ± 0.7 ,³⁹ 30 ± 2.5 ,⁴⁰ and 30.3 ⁴¹ kcal/mol. If we neglect a high value of 35.6 kcal/mol and a low value of 26.5 kcal/mol, the binding energy of atomic carbon based on CO is $Q_C = 174.0$ kcal/mol.

The binding energies reported for CO on Ni(100) are 26.1,⁴² 30.3,⁴³ 30.8,^{44,45} 26.1,⁴⁶ 29.1 ± 0.7 ,³⁹ 27.8,⁴⁷ 28.5,⁴⁸ and 33.1⁴⁹ kcal/mol. They give an average value of $Q_C = 170.7$ kcal/mol, which compares well to 171.5 kcal/mol.³⁶ As will be shown below, the higher the binding energy of carbon, the lower the activation energy of C–C bond scission. Therefore, data on the higher activity of Ni(100) in ethane hydrogenolysis³¹ suggest a higher binding energy of carbon on Ni(100) than on Ni(111). However, this is not the case if CO data are used to calculate Q_C .

If we take all the above values and calculate Q_C using formulas 1a and 2a, then the average value of the carbon binding energy is 171.3 kcal/mol. Taking into account the above arguments, we select this value for the carbon binding energy. We have to neglect structure sensitivity in the calculations and assume that for nickel we have a surface consisting of (111) and (100) planes. Such a decision is also justified by the sensitivity of Q_C to the value of CO the binding energy: a difference of 1.5 kcal/mol for the CO binding energy translates into a difference of about 5 kcal/mol for carbon.

3.1.3. Pd(111). For CO/Pd(111), three very close values are known: 34,^{50,51} 34.8,⁵² and 35.3⁵³ kcal/mol. All values reported for CO/Pd(100) in the literature are noticeably higher, and we had to neglect them. The average value obtained by formula 1a for the carbon binding energy is 189.2 kcal/mol.

3.1.4. Pt(111). For CO/Pt(111) we took 29.6,⁵⁴ 33.0,⁵⁵ 33.0,⁵⁶ 36.7,⁵⁷ 29.2,⁵⁸ and 34.9⁵⁹ kcal/mol, as well as analogous values for CO/Pt(100): 26,⁵⁴ 32.6,⁶⁰ and 27.4⁶¹ kcal/mol. On average, the values for CO/Pt(100) give much lower binding energies; therefore, we used only the above data for the Pt(111) surface and calculated Q_C for this surface: 184.8 kcal/mol.

3.1.5. Ru(0001). For the hcp (0001) surface of ruthenium, three experimental binding energies are known: $Q_{\text{CO}} = 28$ kcal/mol,⁶² $Q_{\text{C}_2\text{H}_2} = 11.6$ kcal/mol,⁶³ and $Q_{\text{C}_2\text{H}_4} = 10–11$ kcal/mol.⁶⁴ The values for acetylene and ethylene binding energies represent much lower binding energies of carbon, which do not agree with each other. They refer to unknown coverages, and we excluded them from consideration. A similar value is known for Ru(1010), $Q_{\text{CO}} = 28$ kcal/mol.⁶⁵ Therefore, we used only one value of CO binding energy for both Ru surfaces: $Q_C = 166.6$ kcal/mol.

3.1.6. Rh(111). The only available value is $Q_{\text{CO}} = 31$ kcal/mol.⁶⁶ This corresponds to $Q_C = 176.8$ kcal/mol. Of course, the use of a single value is statistically unreliable; new data will improve the situation.

3.1.7. Ir(111). For Ir(111), the values of the activation energy of desorption (E_d) and isosteric heats of adsorption (q_{st}) for CO differ by 4–5 kcal/mol. In our calculations we assumed that these values are equal. The following experimental values have been reported: 31.7,⁶⁷ 34,⁶⁸ and 35.8⁶⁹ kcal/mol for E_d ; 35,⁶⁷ 40 (at 0.1–0.3 ML coverages),⁷⁰ and 39⁷¹ kcal/mol for q_{st} . On the average, these values give a binding energy for carbon of 192.7 kcal/mol.

3.1.8. Fe(110). We know of only one experimental value for Fe(110) which can be used here: $Q_{\text{CO}} = 35.8$ kcal/mol.⁷² This corresponds to $Q_C = 192.5$ kcal/mol.

3.1.9. Au(111). The experimental binding energy of a methyl radical to the Au(111) surface is 30 kcal/mol,³⁴ which corresponds to $Q_C = 131.2$ kcal/mol.

3.1.10. Data Correction. The values for carbon binding energies on various surfaces will be used in UBI–QEP calculations of binding energies for other important species in ethane hydrogenolysis (Table 2). In the usual practice, the calculated values are judged against experimental data by assuming that experiments are reliable sources of data whereas calculations use a model that only partially reflects reality. In our opinion, both types of data are error-prone. Most experimental data are indirect and have to be interpreted with

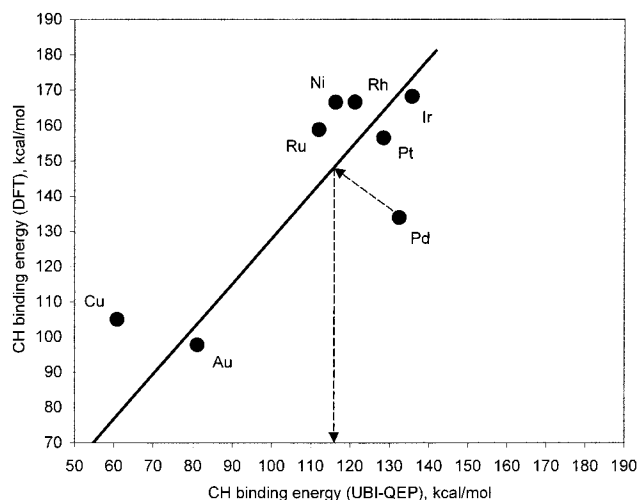


Figure 1. Correlation plot for DFT and UBI–QEP binding energies of CH.

theoretical models and assumptions. The values collected in Table 2 reflect the available experimental data. Those may become more reliable if we find a parameter (a theoretical index) characterizing the metal–carbon binding strength to compare them to. Our attempts to compare the “experimental” binding energies for carbon to simple indices, such as a percentage of *d* character, gave unsatisfactory results.

Unfortunately, we failed to find such an index that could provide reliable information for all the groups VIII and IB metals considered here. The papers by Liao and co-workers are the most complete source of such data.^{73,74} They calculated the binding energies of CH_x on the planes similar to (111) for Ru, Os, Ir, Rh, Ni, Pd, Pt, Cu, Ag, and Au by DFT with transition-state estimates of bond energies (the VWN–B–P functional was used). Quantitatively, these data are unreliable and cannot be used in kinetic modeling. According to these calculations, the binding energies for carbon on the group IB metals are lower than the respective CH binding energies. Unfortunately, Liao et al. did not examine all adsorption modes to identify the most stable of them. The most reliable information is for the CH binding energy since it is plausible that CH binds to a 3-fold cap site on fcc (111) and hcp (0001) planes.⁷⁵ These sites were modeled by two-layer M(3,7) clusters.^{73,74}

Our data correction procedure was as follows. We calculated the binding energy of CH using formula 1 from the binding energies of carbon estimated from the experimental data. Then, we constructed a correlation plot for the CH binding energies obtained by DFT^{73,74} and UBI–QEP (Figure 1).

Because we cannot a priori decide which of the data are more accurate, the corrected values were found as *x*-axis coordinates of the intersection points of the trend line with normals to this line constructed from the points for different atoms (as shown by dashed arrows in Figure 1). The values thus obtained are a compromise with both experiment and theory. Then, the values of carbon binding energies were recalculated from the corrected CH binding energies. The corrected values are listed in the second row of Table 2. In the subsequent developments below we used only the corrected values.

3.1.11. Possible Sources of Errors. As can be seen from the above, Q_{CO} is the main source for calculating Q_C , because most data are for CO. However, the choice of CO molecule is far from ideal. Shustorovich and Sellers believed that the UBI–QEP method is well suited to treat the metal–CO bonding for *3d* metals, such as Cu and Ni, but is inappropriate for *4d* and *5d* metals.²¹ In support of their idea, they cite data from

adsorption calorimetry,⁷⁶ according to which the strength of CO chemisorption at 0.05 ML coverage increases in the series Ni(111) (31 kcal/mol) < Pd(100) (38.9 kcal/mol) < Pt(111) (44.6 kcal/mol); they also claim that the series for carbon is reversed. That is, an increase in CO binding strength occurs together with a decrease in carbon binding strength, which conflicts with UBI–QEP formulas. Thus their conclusion that UBI–QEP is inapplicable to CO chemisorption on *4d* and *5d* metals.

Shustorovich and Sellers added that high-level ab initio calculations could settle the issue, but calculations have not so far, since the DFT–GGA (GGA = generalized gradient approximation) calculations by Hammer et al. for (111) surfaces of these metals project the series Pt (30.3 kcal/mol) < Ni (31.7 kcal/mol) < Pd (33.8 kcal/mol),⁷⁷ and calculations by Kua and Goddard⁷⁸ suggest that Pd (49.45 kcal/mol) > Pt (41.8 kcal/mol). These theoretical data disagree with the calorimetric measurements and doubt the inapplicability of UBI–QEP to CO binding to *4d* and *5d* metals.

In addition, we employed the correction procedure, noncalorimetric data for CO, and some data for other adsorbates assuming that these three sources of data will diminish the possible problems.

Another problem is the use of different sources of experimental values. For instance, we noticed that calorimetric data usually differ substantially from TPD and other data. Therefore, we were selective in the choice of experimental values of adsorbate binding. Most of the other binding, noncalorimetric data are either the activation energies of desorption E_d (which are close to Q in many cases) or isosteric heats of adsorption q_{st} . Those two parameters are often different as is seen from the above Ir(111) data. When calculating E_d from kinetic data, one has to know the preexponential factor of the desorption rate. In some cases, preexponential factors are postulated rather than calculated, and this adds uncertainty.

Theoretically, the heat of adsorption should be almost constant at coverages below 1/3 ML. Experimentally, this is not always true and the zero-coverage value may be higher by 4 kcal/mol (for CO) than the values corresponding to coverages of 0.1–0.3 ML. The reason for such a difference is not yet clear, although some hypotheses exist. In this paper, some zero-coverage values of heats are in fact low-coverage values. Errors may appear because different researchers process their low-coverage values in different manners (some consider the heat to be constant below 1/3 ML, but others consider it to decrease continuously or in a stepwise fashion with an increase in the coverage within this range).

3.2. Binding Energies for Adsorbed Molecules and Radicals. Binding energies were calculated using formulas 1–8 and are compiled in Table 3. The values of physisorption heats for ethane were not calculated by the UBI–QEP method. For Au(111), Table 3 lists the corresponding value taken from experiment.⁷⁹ For Cu(111), we used the value obtained by extrapolating the plot of physisorption energies for *n*-alkanes on Cu(100) vs chain length to ethane.^{79,80} For Pt(111), we used the experimental value.^{79,81,82} For C₂H₆/Rh(111), we chose a value which is 1 kcal/mol higher than the corresponding value for CH₄/Rh(poly).⁸³ For Ru(0001), the value was obtained by extrapolating the plot of physisorption energies for *n*-alkanes on Ru(0001) vs chain length in *n*-alkanes.^{80,84} For Ir(111), the value is experimental.⁸⁵ For Ni(111) and Pd(111) we used the same value as for Pt(111) and Ir(111).

As can be seen from Table 3, all binding energies increase monotonically as the strength of the carbon–metal bond increases. The binding energies of species that bind more

TABLE 3: Binding Energies for CH_x and C₂H_x Calculated Using the UBI–QEP Method and Corrected Values of Carbon Binding Energies

adsorbate	<i>D</i> ^a	Cu(111)	Ni(111)	Pd(111)	Pt(111)	Rh(111)	Ru(0001)	Ir(111)	Au(111)
C		122.9	181.0	170.1	180.6	183.0	175.1	189.6	127.8
CH	81	74.1	125.0	115.2	124.7	126.9	119.7	132.8	78.2
CH ₂	183	49.4	90.0	81.9	89.7	91.5	85.6	96.5	52.6
CH ₃	293	26.7	52.5	47.2	52.3	53.5	49.6	56.8	28.6
CH ₃ –CH ₃	674	6.2	7.7	7.7	7.6	7.0	8.8	7.7	5.7
CH ₃ –CH ₂	576	27.4	53.8	48.4	53.6	54.8	50.8	58.2	29.4
CH ₃ –CH	466	51.0	92.5	84.3	92.2	94.1	88.1	99.1	54.3
CH ₂ –CH ₂	538	8.0	16.8	14.9	16.7	17.1	15.7	18.3	8.6
CH ₃ –C	376	73.4	124.1	114.3	123.7	125.9	118.8	131.9	77.5
CH ₂ –CH	421	11.2	19.2	17.5	19.1	19.5	18.2	20.5	11.8
CH ₂ –C	348	51.1	63.4	61.2	63.3	63.8	62.2	65.1	52.2
CH=CH	392	9.0	18.9	16.8	18.8	19.3	17.7	20.6	9.7
CH=C	259	35.0	43.8	41.9	43.8	44.2	42.8	45.4	35.7
C=C	145	17.7	35.7	32.0	35.0	36.4	33.7	38.8	19.0

^a *D* is the sum of bond energies for the corresponding species in the gas phase.

TABLE 4: Summary of the Calculations for CH_x Chemisorption on Metal Surfaces

metal	<i>Q</i> , kcal/mol				method	note	ref
	C	CH	CH	CH			
Ni(111)	181.0	125.0	90.0	52.5	UBI–QEP		this work
Ni(111)	142.0	128.2	90.2	42.7	DFT	three-layer Ni ₁₃ (7,3,3) cluster	86
Ni(111)	154.0	148.7			DFT	five-layer slab	87, 88
Ni(100)	150	136	91	46	MRCCI		89
Ni(111)	145 ^a	120	88	49	MRCCI		89
Ni(111)				34.1	DFT		90
Pd(111)	170.1	115.2	81.9	47.2	UBI–QEP		this work
Pd(111)	149.3	135.3	85.4	39.9	DFT	two- to three-layer slab	91
Pd(111)		154.1	97.8	50.0	DFT	Pd ₈ cluster	75
Pt(111)	180.6	124.7	89.7	52.3	UBI–QEP		this work
Pt(111)	152.0	166.6	104.3	53.8	DFT	Pt ₈ cluster	75,92
Ru(0001)	175.1	119.7	85.6	49.6	UBI–QEP		this work
Ru(0001)		144.9	90.2	40.4	DFT	Ru ₈ cluster	75
Ru(0001)	164	153.2	97.7	47.4	DFT	four- to five-layer slab	93
Rh(111)	183.0	126.9	91.5	53.5	UBI–QEP		this work
Rh(111)		151.4	98	96.4	DFT	Rh ₈ cluster	75
Ir(111)	189.6	132.8	96.5	56.8	UBI–QEP		this work
Ir(111)		161.4	101.3	50.9	DFT	Ir ₈ cluster	75

^a The value is obtained by extrapolation using the same trend as for Ni(100).

strongly to the surface tend to grow more rapidly. The growth of binding energies is the most pronounced in the case of CH and CH₃C, as well as CH₂ and CH₃CH. The binding energies of these species are the most sensitive to errors in the metal–carbon binding strengths.

3.2.1. *Comparison to other calculations* provides us with interesting information on the trends in the growth of binding energies. This information is summarized in Table 4.

For Ni(111), more information is available than for other metals. Burghgraef et al. carried out quasi-relativistic DFT calculations of three-layer Ni₁₃(7,3,3) clusters using an exchange-correlation potential and a gradient-corrected exchange energy functional in combination with the Stoll correction for correlation.⁸⁶ They obtained preferred coordinations for CH₃ (top), CH₂ (cap), CH (cap), and C (cap). These data are compared in Figure 2. Klinke et al. carried out five-layer slab calculations of the C/Ni(111)⁸⁷ and CH/Ni(111)⁸⁸ systems using DFT within the generalized gradient approximation and the FP–LAPW method. These calculations corresponded to 0.25 ML coverage, at which the values of binding energies are virtually indistinguishable from zero-coverage values. Siegbahn and Panas performed MRCCI calculations⁸⁹ with bond-prepared clusters of 10–20 atoms. These data are in excellent agreement with values reported by Burghgraef⁸⁶ and in good agreement with our data. Michaelides and Hu found that CH₃ prefers a 3-fold site and binds with an energy of 34.1 kcal/mol (compare to 52.5 kcal/

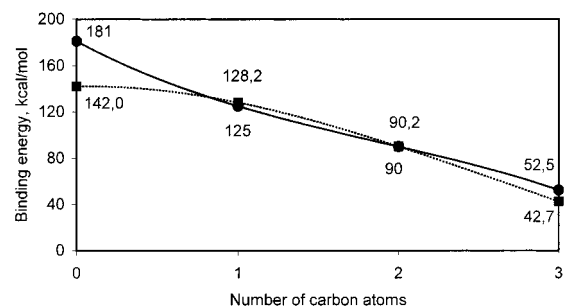


Figure 2. Trends in binding energies for CH_x/Ni(111) calculated by UBI–QEP (solid line) and DFT⁸⁶ (dashed line) methods.

mol obtained in this work).⁹⁰ This value was obtained by DFT–gradient-corrected spin-polarized calculations. The best agreement between UBI–QEP and other calculations is observed for CH and CH₂ species. The UBI–QEP binding energy for CH₃ is higher by 3–9 kcal/mol. A deviation of 35–37 kcal/mol for carbon binding is very high.

For Pd(111), Paul and Sautet carried out DFT calculations with a GGA PW91 functional.⁹¹ They considered a surface coverage of 1/3 ML. These are very close to the corresponding values for the Ni(100) surface.⁸⁹ Kua et al. reported analogous values for CH, CH₂, and CH₃ calculated for M₈ clusters using DFT (B3LYP) and their interstitial electron surface model for the zero-coverage limit.⁷⁵ Figure 3 compares slab and cluster

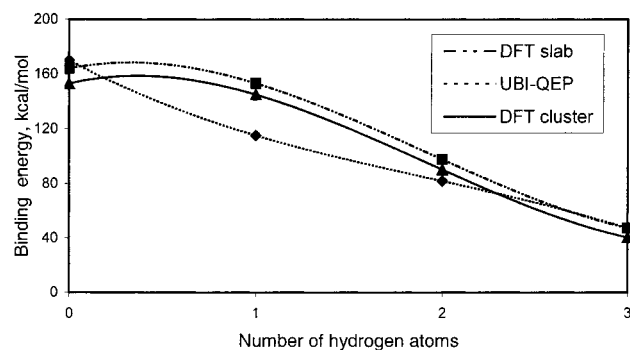


Figure 3. Trends in binding energies for $\text{CH}_x/\text{Pd}(111)$, calculated by UBI-QEP and DFT.^{75,91}

DFT calculations to the results of this work. As can be seen, the results obtained by the slab model are closer to the UBI-QEP values.

For Pt(111), Kua and Goddard^{75,92} obtained the data for M_8 clusters using DFT (B3LYP) and the interstitial electron surface model. The binding energies for CH_3 (top), CH_2 (bridge), CH (cap), and C (cap) compare unfavorably to the UBI-QEP data. According to the DFT data, the total bond energy to the surface is proportional to the number of Pt–C bonds (53 ± 3 kcal/mol per bond). This trend conflicts with the bond-order conservation approach underlying the UBI-QEP model. It is also noteworthy that carbon binds to Pt(111) less strongly than CH. Other binding energies are also different. DFT predicts a more rapid growth of the binding energy with an increase in the number of bonds to the surface.

For Ru(0001), two sources of data in addition to UBI-QEP are available. Kua et al. reported DFT-calculated binding

energies for CH, CH_2 , and CH_3 .⁷⁵ Ciobica et al. also studied CH_x chemisorption on this surface using DFT (periodical calculations, GGA, and the Perdew-Wang 91 functional).⁹³ They are compared in Table 4. These three sets of data (DFT-cluster, DFT-slab, and UBI-QEP) are very different, but the DFT-cluster and DFT-slab data follow the same trend: the energies obtained using the slab model of the surface are just 7–9 kcal/mol higher.

For Rh(111) and Ir(111), the only source of theoretical data is a paper by Kua et al.⁷⁵ In both cases, the DFT binding energies of CH and CH_2 are higher than for UBI-QEP, but lower in the case of CH_3 . To summarize the results obtained by Kua et al.,⁷⁵ we note that their data suggest the following activity series for C–C bond scission: Pt(111) > Ir(111) > Os(0001) \approx Pd(111) > Rh(111) > Ru(0001). This series is different from the experimental trend Ir(111) > Ru(0001) > Pt(111).¹⁹ Our data compare more favorably with the experimental series Ir(111) > Ni(111) \approx Pt(111) > Ru(0001), although the placement of ruthenium is still inadequate.

In addition to DFT calculations, attempts have been made to estimate carbon–metal binding strengths using the polar covalence model (PCM) developed by Sanderson and applied by Frese to binding on surfaces.⁹⁴ This model predicts lower binding energies than UBI-QEP and DFT, but the qualitative agreement with our findings is excellent. Thus, UBI-QEP binding energies of atomic carbon increased within the series Pd < Ru < Pt \approx Ni < Ir < Fe, whereas the PCM projection is Pd < Pt \approx Ru < Ni \approx Ir < Fe. It is highly improbable that this qualitative similarity is accidental.

3.2.2. Trends in Binding Energies. The DFT and UBI-QEP binding energies for CH_x follow radically different trends. In

TABLE 5: Activation Energies and Enthalpies of C–C Bond Scission Steps

reaction ^a	D ^b	Cu(111)	Ni(111)	Pd(111)	Pt(111)	Rh(111)	Ru(0001)	Ir(111)	Au(111)
Forward Activation Energy									
$\text{CH}_3\text{CH}_3 \rightarrow \text{CH}_3 + \text{CH}_3$	88	40.8	8.5	12.5	8.6	7.4	11.2	5.3	25.4
$\text{CH}_3\text{CH}_2 \rightarrow \text{CH}_3 + \text{CH}_2$	100	51.3	22.2	24.6	11.6	21.8	23.5	20.3	48.2
$\text{CH}_3\text{CH} \rightarrow \text{CH}_3 + \text{CH}$	92	42.2	22.0	23.7	22.1	21.7	22.9	20.6	39.4
$\text{CH}_2\text{CH}_2 \rightarrow \text{CH}_2 + \text{CH}_2$	172	81.2	26.9	32.0	9.3	25.9	29.7	22.8	75.5
$\text{CH}_3\text{C} \rightarrow \text{CH}_3 + \text{C}$	83	14.3	7.2	8.5	7.2	6.9	7.9	6.1	13.7
$\text{CH}_2\text{CH} \rightarrow \text{CH}_2 + \text{CH}$	157	44.8	6.7	12.6	6.9	5.6	9.9	2.0	38.1
$\text{CH}_2\text{C} \rightarrow \text{CH}_2 + \text{C}$	165	43.8	8.8	14.8	9.0	7.7	12.0	4.0	36.9
$\text{CHCH} \rightarrow \text{CH} + \text{CH}$	230	90.9	30.6	37.0	30.9	29.5	34.1	25.7	83.3
$\text{CHC} \rightarrow \text{CH} + \text{C}$	178	16.1	0.0	1.7	0.0	0.0	0.0	0.0	28.1
$\text{CC} \rightarrow \text{C} + \text{C}$	145	0.0	0.0	0.0	0.0	0.0	0.0	0.0	0.0
Enthalpy									
$\text{CH}_3\text{CH}_3 \rightleftharpoons \text{CH}_3 + \text{CH}$	88	40.8	−9.2	1.4	−8.9	−11.9	−2.3	−17.9	36.4
$\text{CH}_3\text{CH}_2 \rightleftharpoons \text{CH}_3 + \text{CH}_2$	100	51.3	11.3	19.2	11.6	9.8	15.6	4.9	48.2
$\text{CH}_3\text{CH} \rightleftharpoons \text{CH}_3 + \text{CH}$	92	42.2	7.0	13.9	7.3	5.8	10.8	1.5	39.4
$\text{CH}_2\text{CH}_2 \rightleftharpoons \text{CH}_2 + \text{CH}_2$	172	81.2	8.8	23.0	9.3	6.1	16.5	−2.7	75.5
$\text{CH}_3\text{C} \rightleftharpoons \text{CH}_3 + \text{C}$	83	6.7	−26.4	−19.9	−26.1	−27.6	−22.9	−31.5	4.0
$\text{CH}_2\text{CH} \rightleftharpoons \text{CH}_2 + \text{CH}$	157	44.8	−38.9	−22.7	−38.3	−41.9	−30.1	−51.8	38.1
$\text{CH}_2\text{C} \rightleftharpoons \text{CH}_2 + \text{C}$	165	43.8	−42.6	−25.8	−42.0	−45.7	−33.5	−56.0	36.9
$\text{CHCH} \rightleftharpoons \text{CH} + \text{CH}$	230	90.9	−1.2	16.3	−0.6	−4.4	8.3	−15.1	83.3
$\text{CHC} \rightleftharpoons \text{CH} + \text{C}$	178	16.1	−84.2	−65.4	−83.5	−87.7	−74.0	−99.0	7.7
$\text{CC} \rightleftharpoons \text{C} + \text{C}$	145	−83.1	−181.3	−163.2	−180.6	−184.6	−171.5	−195.4	−91.6
Backward Activation Energy									
$\text{CH}_3 + \text{CH}_3 \rightarrow \text{CH}_3\text{CH}_3$	88	0.0	17.7	11.1	17.5	19.3	13.6	23.1	0.0
$\text{CH}_3 + \text{CH}_2 \rightarrow \text{CH}_3\text{CH}_2$	100	0.0	10.9	5.3	0.0	12.0	7.9	15.4	0.0
$\text{CH}_3 + \text{CH} \rightarrow \text{CH}_3\text{CH}$	92	0.0	15.0	9.8	14.8	15.9	12.1	19.1	0.0
$\text{CH}_2 + \text{CH}_2 \rightarrow \text{CH}_2\text{CH}_2$	172	0.0	18.1	9.0	0.0	19.8	13.2	25.4	0.0
$\text{CH}_3 + \text{C} \rightarrow \text{CH}_3\text{C}$	83	7.6	33.5	28.4	33.3	34.5	30.8	37.6	9.7
$\text{CH}_2 + \text{CH} \rightarrow \text{CH}_2\text{CH}$	157	0.0	45.6	35.3	45.2	47.5	40.0	53.8	0.0
$\text{CH}_2 + \text{C} \rightarrow \text{CH}_2\text{C}$	165	0.0	51.4	40.6	51.0	53.3	45.5	60.0	0.0
$\text{CH} + \text{CH} \rightarrow \text{CHCH}$	230	0.0	31.9	20.6	31.5	33.9	25.8	40.8	0.0
$\text{CH} + \text{C} \rightarrow \text{CHC}$	178	0.0	84.2	67.0	83.5	87.7	74.0	99.0	20.4
$\text{C} + \text{C} \rightarrow \text{CC}$	145	83.1	181.3	163.2	180.6	184.6	171.5	195.4	91.6

^a All species are adsorbed on the surface. ^b Dissociation enthalpy.

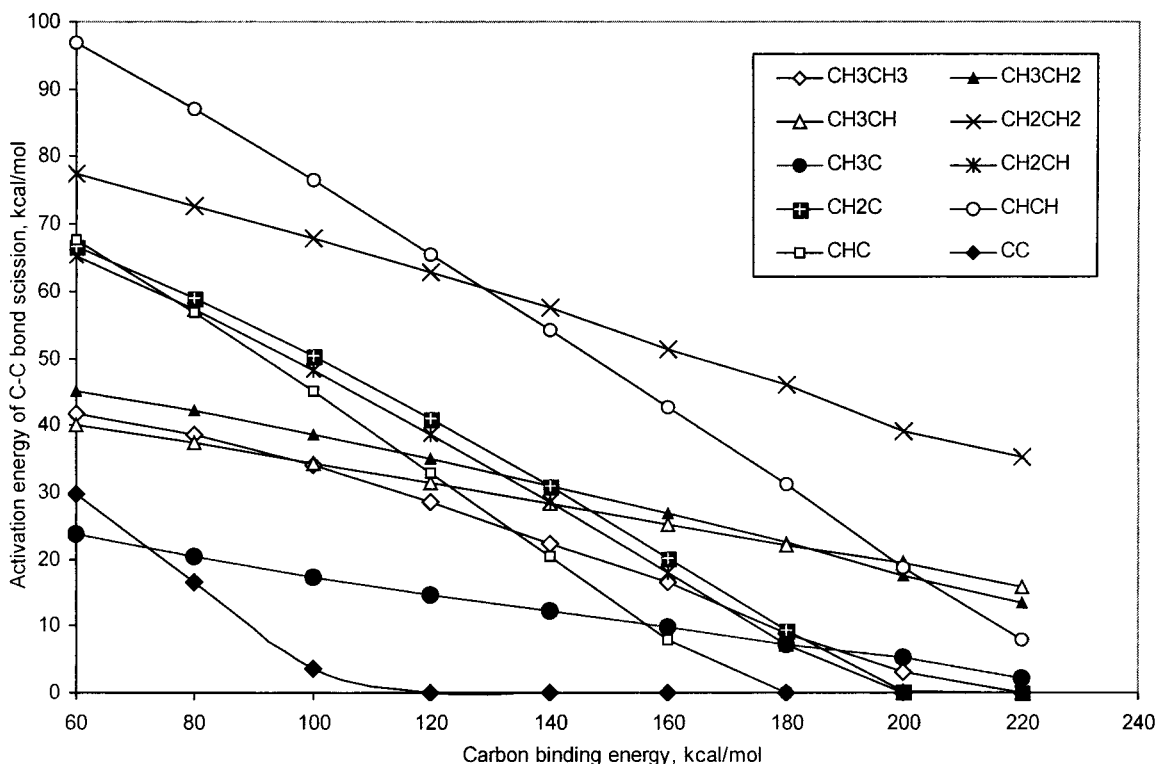


Figure 4. Activation energies of C–C bond scission steps vs binding energy of the carbon atom. The legend to this figure shows the immediate precursors of C–C bond scission.

both cases, the curves of binding energies vs number of hydrogen atoms in CH_x can be approximated by the third- or fourth-order polynomials with alternating positive and negative coefficients. However, the signs of coefficients alternate “in different phases”. Whenever a coefficient is positive for DFT, it is negative for UBI–QEP and vice versa. The DFT binding energies increase roughly in proportion to the number of bonds formed between an adsorbate and the surface. That is why binding energies for C and CH in cap sites are close (compare a binding energy of 152 kcal/mol for carbon on Pt(111) and a binding energy of 166.6 kcal/mol for CH).⁹² The UBI–QEP binding energies increase roughly in proportion to the number of bonds that might be formed if the contact atom(s) of an adsorbate employs all its coordination vacancies (if we take 152 kcal/mol for C, then we obtain 99.2 kcal/mol for CH). Therefore, the best agreement between DFT and UBI–QEP is reached when the contact atoms use all of their valencies. A priori it is difficult to choose between the two schemes because no clear reference points are available; the scatters of experimental data are too broad.

3.3. Activation Energies of C–C Bond Scission Steps.

Blowers and Masel examined the accuracy of the bond-order conservation assumption in the case of some gas-phase hydrogenolysis and dehydrogenation reactions.⁹⁵ They concluded that, although bond-order conservation does not predict the correct transition-state geometry, the energies of the transition state predicted with bond-order-conserved pathways are very close to their ab initio values. Ab initio predictions at the MP2(full)/6-31G* level and bond-order conservation predictions for barrier energies differ by only 1–2 kcal/mol. So given the “correct binding energies”, the activation energies of elementary steps in multistep reactions are predicted very accurately.

We calculated the activation energies using formulas 9–12. The resulting data are summarized in Table 5. In fact, within

the UBI–QEP method, a higher carbon binding strength automatically means a lower activation energy of C–C bond scission.²⁰

If the activity of metal surfaces toward ethane hydrogenolysis is estimated by the values of activation energies in C–C bond scission steps, then the metals can be arranged in the following activity series:⁹⁶ $\text{Cu}(111) < \text{Au}(111) < \text{Pd}(111) < \text{Ru}(0001) < \text{Pt}(111) \approx \text{Ni}(111) < \text{Rh}(111) < \text{Ir}(111) < \text{Fe}(110)$. If the correction described above were not introduced, the activity series would be $\text{Cu}(111) < \text{Au}(111) < \text{Ru}(0001) < \text{Ni}(111) < \text{Rh}(111) < \text{Pt}(111) < \text{Pd}(111) < \text{Fe}(110) \approx \text{Ir}(111)$.

It is likely that the activity of iron is not determined by its capability to break C–C bonds. In fact, this step is not rate-determining in ethane hydrogenolysis for this metal.¹⁵ In the case of a real supported iron catalyst, a carbonaceous layer is probably formed, which leads to site blocking and a decrease in activity toward hydrogenolysis. This may explain why iron is inactive.¹ The fact that Ir is the most active in the series agrees with the experimental data.¹⁹ This is not the case if we employ DFT binding energies.⁷⁵ The low activities of the group IB metals are also in agreement with observations.^{1,2}

However, there are also disagreements with observations. Thus, our data suggest that Ni is not less active than Ru, and this conflicts with experiment. Probably, the relative chemisorption strengths suggested by the CO chemisorption data on Ni and Ru used in this work are in error. The relative positions of Ru and Ni in the periodic table are also suggestive of the higher chemisorption strength of Ru. A relatively high activity of Pt predicted by both UBI–QEP and DFT contradicts experiment.

Both chemisorption heats of species adsorbed via carbon atoms and the activation energies of reactions between these species largely depend on the binding energies of carbon on metal surfaces, which are needed for UBI–QEP calculations. Figure 4 illustrates this dependence. The activation energy of

C–C bond scission in intermediates bound to the surface via two or more metal atoms is more sensitive to the carbon binding energies than that of intermediates bound to the surface via one atom. This means that, if one proves that C–C scission in ethylidene, ethylidene, and ethyl is an important step for ethane hydrogenolysis on one of the metals, than for any other similar metal, this step should be taken into account as well. Conversely, the necessity of taking into account C–C bond scission in C_2H_2 (ads) or C_2H_4 (ads) for one metal does not imply that this step will occur on other metals.

For groups VIII and IB metals, the heat of carbon adsorption is within the limits of 120–200 kcal/mol. Steps with activation energies higher than 50–60 kcal/mol virtually do not occur. Therefore, we can restrict ourselves to considering the steps and metals within these limits (Figure 4). As can be seen the scission of C–C bonds in hydrogen-free C_2 species occurs without an activation energy. In most cases, C–C bond scission probably occurs before the complete dehydrogenation of ethane because this step is thought of as being rate-determining in most cases.

After C_2 , the most active species in C–C bond scission are ethylidyne and CHC. The following species have moderate activation energies in C–C bond scission: CH_3CH_3 , CH_2CH , CH_2C , CH_3CH , and CH_3CH_2 . Adsorbed acetylene and ethylene have the highest activation energies. It is somewhat odd that the C–C bond cleaves easier in ethane than in acetylene and ethylene. Probably, the UBI–QEP model underestimates the activation energies when the reaction is sterically hindered. The activation energy of acetylene may be somewhat overestimated because the model considers the $M-C\equiv C-M$ type of adsorption, whereas quad- σ -bonded and π /di- σ -bonded acetylene may also be formed; for them, the activation energies of C–C bond scission should be lower because these two types of acetylene adsorption correspond to higher binding energies. C–C bond scission in ethylene is more probable in the case of metals capable of stronger chemisorption.

In all cases, a C–C bond cleaves more readily if a metal forms stronger chemical bonds with carbon atoms. The stability of species on these metals is also higher on such surfaces. However, hydrogenolysis is known to be sensitive to carbonaceous deposits on the catalyst surface, and such deposits are readily formed on strongly chemisorbing surfaces. Therefore, there should be an optimal metal–carbon bond strength: high enough to favor C–C bond scission and low enough to prevent blocking of the surface by deposits. If this optimum does not match any known metal, the best catalyst could be found by designing an alloyed or doped metal surface.

As can be seen from Figure 4, asymmetric species on the surface break C–C bonds more readily: CH_2C is more active than C_2H_2 , and CH_3C is more active than CH_2CH . The degree of dehydrogenation has a nontrivial effect on the activation energy. In some cases, the smaller the number of hydrogen atoms, the lower the activation energy, as in the case of CH_3C , CH_3CH , and CH_3CH_2 . In other cases, the relative activities depend on metal–carbon bond strengths.

In the range of carbon binding energies between 140 and 180 kcal/mol, UBI–QEP predicts the following activity series for the possible intermediates in ethane hydrogenolysis: $CC > CHC, CH_3C > CH_2CH > CH_2C > CH_3CH > CH_3CH_2 > CHCH > CH_2CH_2$.

4. Conclusions

The binding energies of CH_x and C_2H_x species on the Ni(111), Pd(111), Pt(111), Rh(111), Ru(001), Ir(111), Fe(110),

Cu(111), and Au(111) surfaces and the activation energies of C–C bond scission can be estimated from the binding energy of atomic carbon on these surfaces. The strength of carbon binding is estimated from the experimental adsorption energies of various species. We find that metal surfaces can be arranged in order of increasing binding strength: $Cu(111) < Au(111) < Pd(111) < Ru(001) < Pt(111) \approx Ni(111) < Rh(111) < Ir(111) < Fe(110)$. The activity of these surfaces toward C–C bond scission increases in the same series. UBI–QEP alone does not allow us to draw definitive conclusions on the mechanism of ethane hydrogenolysis, although CC, CHC, and CH_3C can be thought of as the most active species in C–C bond scission.

Acknowledgment. We thank Irena Efremenko (Department of Chemical Engineering, Technion–Israel Institute of Technology, Haifa) for useful remarks after reading the manuscript prior to submission. R.E.V.P. was supported in part by grant IIS-9988084 from the U.S. National Science Foundation. This research was sponsored in part by a NATO Collaborative Research Grant.

References and Notes

- (1) Sinfelt, J. H. *Adv. Catal.* **1973**, *23*, 91.
- (2) Sinfelt, J. H. *Catal. Rev.* **1970**, *3*, 175.
- (3) Sinfelt, J. H. *J. Catal.* **1972**, *27*, 468.
- (4) (a) Goddard, S. A.; Amiridis, M. D.; Rekoske, J. E.; Cardona-Martinez, N.; Dumesic, J. A. *J. Catal.* **1989**, *117*, 155. (b) Dumesic, J. A.; Rudd, D. F.; Aparicio, L. M.; Rekoske, J. E.; Treviño, A. A. *The Microkinetics of Heterogeneous Catalysis*; American Chemical Society: Washington, DC, 1993; Chapter 7.
- (5) Bond, G. C.; Hooper, A. D.; Slaa, J. C.; Taylor, A. O. *J. Catal.* **1996**, *163*, 319.
- (6) Guzzi, L.; Gudkov, B. S.; Tetenyi, P. *J. Catal.* **1972**, *24*, 187.
- (7) Tanaka, K.; Miyazaki, T.; Aomura, K. *J. Catal.* **1983**, *81*, 328.
- (8) Smale, M. W.; King, T. S. *J. Catal.* **1990**, *125*, 335.
- (9) Gudkov, B. S.; Guzzi, L.; Tetenyi, P. *J. Catal.* **1982**, *74*, 207.
- (10) Engstrom, J. R.; Goodman, D. W.; Weinberg, W. H. *J. Am. Chem. Soc.* **1988**, *110*, 8305.
- (11) Rodriguez, J. A.; Goodman, D. W. *J. Phys. Chem.* **1990**, *94*, 5342.
- (12) Martin, G. A. *J. Catal.* **1979**, *60*, 345.
- (13) Wang, P.-K.; Slichter, C. P.; Sinfelt, J. H. *J. Phys. Chem.* **1990**, *94*, 1154.
- (14) Ko, E. I.; Garten R. L. *J. Catal.* **1981**, *68*, 233.
- (15) Frennet, A.; Degols, L.; Lienard, G.; Crucq, A. *J. Catal.* **1974**, *35*, 18.
- (16) Boudart, M. *AIChE J.* **1972**, *18*, 465.
- (17) Mahaffy P.; Hansen R. S. *J. Chem. Phys.* **1979**, *71*, 1853.
- (18) Chen B.; Goodwin J. G., Jr. *J. Catal.* **1995**, *154*, 1.
- (19) Rodriguez, J. A.; Goodman, D. W. *Surf. Sci. Rep.* **1991**, *14*, 1.
- (20) Shustorovich, E. *Adv. Catal.* **1990**, *37*, 101.
- (21) Shustorovich, E.; Sellers, H. *Surf. Sci. Rep.* **1998**, *31*, 1.
- (22) *CRC Handbook of Chemistry and Physics*; Robert, C. W., Ed.; CRC Press: Boca Raton, FL, 1985–1986.
- (23) Bradford, M. C. *J. Catal.* **2000**, *189*, 238.
- (24) Benziger, J. B. In *Metal-Surface Reaction Energetics: Theory and Applications to Heterogeneous Catalysis, Chemisorption and Surface Diffusion*; Shustorovich, E., Ed.; VCH: New York, 1991; p 53.
- (25) Lin, J.-L.; Bent, B. E. *J. Phys. Chem.* **1993**, *97*, 9713.
- (26) Hollins, P.; Pritchard J. *Surf. Sci.* **1979**, *89*, 486.
- (27) Peterson, L. D.; Kevan, S. D. *J. Chem. Phys.* **1991**, *94*, 2281.
- (28) Tracy, J. C. *J. Chem. Phys.* **1972**, *56*, 2748. The value used in this paper corresponds to coverages of 0.1–0.5 ML. The value obtained by extrapolating to zero coverage is unexpectedly high (about 16 kcal/mol). A general trend is that the value at a very low coverage is very high due to reasons that are not yet clear (surface reconstruction, defect sites, and stepped sites are often considered as possible reasons). Then, the coverage remains virtually constant up to $\sim 1/3$ ML.
- (29) Yang, M. X.; Bent, B. E. *J. Phys. Chem.* **1996**, *100*, 822.
- (30) Jenks, C. J.; Xi, M.; Yang, M. X.; Bent, B. E. *J. Phys. Chem.* **1994**, *98*, 2152.
- (31) Goodman, D. W. *Surf. Sci.* **1982**, *123*, L697.
- (32) Shustorovich, E.; Bell, A. T. *Surf. Sci.* **1991**, *248*, 359.
- (33) Shustorovich, E.; Bell, A. T. *Surf. Sci.* **1991**, *253*, 386.
- (34) Paredes-Oliveira, P.; Patrino, E. M.; Sellers, H. *Surf. Sci.* **1995**, *327*, 330.

- (35) Hei, M. J.; Chen, H. B.; Yi, J.; Lin, Y. J.; Lin, Y. Z.; Wei, G.; Liao, D. W. *Surf. Sci.* **1998**, *417*, 82.
- (36) Isett, L. C.; Blakeley, J. N. *Surf. Sci.* **1975**, *47*, 645.
- (37) Christmann, K.; Schober, O.; Ertl, G. *J. Chem. Phys.* **1974**, *60*, 4719.
- (38) Ibach, H.; Erley, W.; Wagner, H. *Surf. Sci.* **1980**, *92*, 29.
- (39) Stuckless, J. T.; Al-Sarraf, N.; Wartnaby, C. E.; King, D. A. *J. Chem. Phys.* **1993**, *99*, 2202.
- (40) Miller, J. B.; Siddiqui, H. R.; Gates, S. M.; Hagans, P. L.; Yates, J. T., Jr. *J. Chem. Phys.* **1987**, *87*, 6725.
- (41) Froitzheim, H.; Köhler, U. *Surf. Sci.* **1987**, *188*, 70.
- (42) Johnson, S.; Madix, R. J. *Surf. Sci.* **1981**, *108*, 77.
- (43) Boszo, F.; Ertl, G.; Grunze, M.; Weiss, M. *Appl. Surf. Sci.* **1977**, *1*, 103.
- (44) Bordoli, R. S.; Vickerman, J. C.; Wolsteholm, J. *Surf. Sci.* **1979**, *85*, 244.
- (45) Labohm, F.; Engelen, C. W. R.; Gijzeman, O. L. J.; Geus, J. W.; Bootsma, G. A. *J. Chem. Soc., Faraday Trans. 1* **1982**, *78*, 2435.
- (46) Klier, K.; Zettlemoyer, A. C.; Leidheiser, H., Jr. *J. Chem. Phys.* **1970**, *52*, 589.
- (47) Benziger, J. B.; Madix, R. J. *Surf. Sci.* **1979**, *79*, 394.
- (48) Kiskinova, M.; Goodman, D. W. *Surf. Sci.* **1981**, *108*, 64.
- (49) Koel, B. E.; Peebles, D. E.; White, J. M. *Surf. Sci.* **1983**, *125*, 709.
- (50) Ertl, G.; Koch, J. *Z. Naturforsch., A* **1970**, *25*, 1906.
- (51) Conrad, H.; Ertl, G.; Koch, J.; Latta, E. E. *Surf. Sci.* **1974**, *43*, 462.
- (52) Szanyi, J.; Kuhn, W. K.; Goodman, D. W. *J. Phys. Chem.* **1994**, *98*, 2978.
- (53) Voogt, E. H.; Coulier, L.; Gijzeman, O. L. J.; Geus, J. W. *J. Catal.* **1997**, *169*, 359.
- (54) McCabe, R. W.; Schmidt, L. D. *Surf. Sci.* **1977**, *66*, 101.
- (55) Ertl, G.; Neumann, M.; Streit, K. M. *Surf. Sci.* **1977**, *64*, 393.
- (56) Sexton, B. A.; Rendulic, K. D.; Hughes, A. E. *Surf. Sci.* **1982**, *121*, 181.
- (57) Shigeishi, R. A.; King, D. A. *Surf. Sci.* **1976**, *58*, 379.
- (58) Lee, W. T.; Ford, L.; Blowers, P.; Nigg, H. L.; Masel, R. I. *Surf. Sci.* **1998**, *416*, 141.
- (59) Campbell, C. T.; Ertl, G.; Kuipers, H.; Segner, J. *J. Chem. Phys.* **1980**, *73*, 5862.
- (60) Küppers, J.; Michel, H. *J. Vac. Sci. Technol.* **1976**, *13*, 259.
- (61) Thiel, P. A.; Behm, R. J.; Norton, P. R.; Ertl, G. *J. Chem. Phys.* **1983**, *78*, 7448.
- (62) Madey, T. E.; Menzel, D. *Jpn. J. Appl. Phys.* **1974**, Suppl. 2, Part 2, 841.
- (63) Hills, M. M.; Parmeter, J. E.; Mullins, C. B.; Weinberg, W. H. *J. Am. Chem. Soc.* **1986**, *108*, 3554.
- (64) Parmeter, J. E.; Hills, M. M.; Weinberg, W. H. *J. Am. Chem. Soc.* **1987**, *109*, 72.
- (65) Reed, P. D.; Comrie, C. M.; Lambert, R. M. *Surf. Sci.* **1976**, *59*, 33.
- (66) Castner, D. G.; Sexton, B. A.; Somorjai, G. A. *Surf. Sci.* **1978**, *71*, 519.
- (67) Comrie, C. M.; Weinberg, W. H. *J. Chem. Phys.* **1976**, *64*, 250.
- (68) Küppers, J.; Plagge, A. *J. Vac. Sci. Technol.* **1976**, *13*, 259.
- (69) (a) Lauterbach, J.; Boyle R. W.; Schick, M.; Mitchell W. J.; Meng, B.; Weinberg, W. H. *Surf. Sci.* **1996**, *350*, 32. (b) Sushchikh, M.; Lauterbach, J.; Weinberg, W. H. *Surf. Sci.* **1997**, *393*, 135.
- (70) Boyle, R. W.; Lauterbach, J.; Schick, M.; Mitchell W. J.; Weinberg, W. H. *Ind. Eng. Chem. Res.* **1996**, *35*, 2986.
- (71) Hagen, D. I.; Nieuwenhuys, B. E.; Rovida, G.; Somorjai, G. A. *Surf. Sci.* **1976**, *57*, 632.
- (72) Wedler, G.; Ruhmann, H. *Surf. Sci.* **1982**, *121*, 464.
- (73) Au, C.-T.; Ng, C.-F.; Liao, M.-S. *J. Catal.* **1999**, *185*, 12.
- (74) Liao, M.-S.; Zhang, Q.-E. *J. Mol. Catal., A* **1998**, *136*, 185.
- (75) Kua, J.; Faglioni, F.; Goddard, W. A., III. *J. Am. Chem. Soc.* **2000**, *122*, 2309.
- (76) Brown, W. A.; Kose, R.; King, D. A. *Chem. Rev.* **1998**, *98*, 797.
- (77) Hammer, B.; Morikawa, Y.; Nørskov, J. K. *Phys. Rev. Lett.* **1996**, *76*, 2141.
- (78) Kua, J.; Goddard, W. A., III. *J. Am. Chem. Soc.* **1999**, *121*, 10928.
- (79) Wetterer, S. M. Helium Atom Reflectivity Study of Physisorption and Chemisorption on Single Crystal Metal Surfaces. Ph.D. Thesis, Princeton University, Princeton, NJ, 1998.
- (80) Kubota, J.; Ichihara, S.; Kondo, J. N.; Domen, K.; Hirose, C. *Surf. Sci.* **1996**, *357/358*, 634.
- (81) McMaster, M. C.; Arumainayagam, C. R.; Madix, R. J. *Chem. Phys.* **1993**, *177*, 461.
- (82) Arumainayagam, C. R.; Schoofs, G. R.; McMaster, M. C.; Madix, R. J. *J. Phys. Chem.* **1991**, *95*, 1041.
- (83) Brass, S. G.; Ehrlich, G. *Surf. Sci.* **1987**, *187*, 21.
- (84) Brand, J. L.; Arena, M.; Deckert, A. A.; George, S. M. *J. Chem. Phys.* **1990**, *92*, 5136.
- (85) Johnson, D. F.; Weinberg, W. H. *J. Chem. Phys.* **1995**, *103*, 5833.
- (86) Burghgraef, H.; Jansen, A. P. J.; van Santen, R. A. *Surf. Sci.* **1995**, *324*, 345.
- (87) Klinke, D. J., II; Wilke, S.; Broadbelt, L. J. *J. Catal.* **1998**, *178*, 1998.
- (88) Klinke, D. J., II; Dooling D. J.; Broadbelt L. J. *Surf. Sci.* **1999**, *425*, 334.
- (89) Siegbahn, P. E. M.; Panas, I. *Surf. Sci.* **1990**, *240*, 37.
- (90) Michaelides, A.; Hu, P. *Surf. Sci.* **1999**, *437*, 362.
- (91) Paul, J.-F.; Sautet, P. *J. Phys. Chem. B* **1998**, *102*, 1678.
- (92) Kua, J.; Goddard, W. A., III. *J. Chem. Phys. B* **1998**, *102*, 942.
- (93) Ciobăcă, I. M.; Frechard, F.; van Santen, R. A.; Kley, A. W.; Hafner, J. *Chem. Phys. Lett.* **1999**, *311*, 185.
- (94) Frese, K. W., Jr. *Surf. Sci.* **1987**, *182*, 85.
- (95) Blowers, P.; Masel, R. *Surf. Sci.* **1998**, *417*, 238.
- (96) Estimating the activities of metal surfaces from their activities in C–C bond scission steps may appear incorrect because different surfaces might prefer different intermediates as scission precursors and because C–C bond scission is not necessarily a rate-determining step.